

Evaluation of Ultra-High-Speed Line Protection, Traveling-Wave Fault Locating, and Circuit Breaker Reignition Detection on a 220 kV Line in the Kalahari Basin, Namibia

Frans Shanyata, *NamPower*

Sthitaprajnyan Sharma, Deon Joubert, Richard Kirby, and Greg Smelich,
Schweitzer Engineering Laboratories, Inc.

Abstract—*NamPower is the national power utility company of Namibia and owns a world-class transmission and distribution network, which is one of the longest of its kind in the world. NamPower installed ultra-high-speed (UHS) relays to monitor one of the two 220 kV, 113.6 km (70.59 mi) overhead lines between Omburu and Khan substations to evaluate the performance of the line protection and accuracy of traveling-wave-based fault locating (TWFL).*

Index Terms—*Traveling waves, power system, line protection, UHS line protection, UHS relays, fault-clearing time, critical fault-clearing time, fault locating, and transient stability.*

I. INTRODUCTION

NamPower is Namibia’s national power utility, originally known as South West Africa Water and Electricity Corporation (SWAWEK). The key to SWAWEK’s success was the effective development of the Ruacana hydropower station (the Ruacana Scheme with a capacity of 240 MW installed in 1978) and the establishment of a transmission system for the distribution of electricity through the country’s central districts to Windhoek. In its 32-year history, SWAWEK has made valuable contributions to the country’s economic development. In July 1996, SWAWEK became NamPower. Today, NamPower’s 34,000 km transmission and distribution network is one of the longest networks in the world. The transmission network includes transmission lines at voltage levels from 66 kV to 400 kV ac and 350 kV high-voltage dc transmission link (HVdc).

This paper explains in detail the observations and experiences gained from the evaluation of the ultra-high-speed (UHS) relays for a C-phase-to-ground fault that occurred on the 220 kV Omburu-Khan 1 line on February 4, 2020. Section II describes the NamPower system, the 220 kV Omburu-Khan 1 line, and NamPower’s standard line protection philosophy.

Section III elaborates on the event analysis of the internal fault on February 4, 2020. The analysis aims to correlate the concepts of UHS protection and TWFL to their actual performance in the field using the transient records captured during this fault. Section IV compares fault-clearing time of UHS relays with existing phasor-based relays and the potential capabilities of UHS protection to aid with system stability and critical clearing time. Section V provides additional observations from the 1 MHz transient records, such as breaker reignition and post-fault arcing, which aid asset management and preventive maintenance.

II. THE NAMPOWER SYSTEM

NamPower owns and operates three power stations with the combined installed capacity of 459.50 MW. The following power stations are the main sources of local power generation capacity in the country:

- 347 MW Ruacana hydroelectric power station in the Kunene region
- 90 MW Van Eck coal-fired power station outside of Windhoek
- 22.5 MW Anixas diesel-powered power station at Walvis Bay

NamPower owns a world-class transmission system and a network of 66 kV to 400 kV overhead lines spanning more than 11,704 km (shown in Fig. 1). Continuous investments are made to strengthen and keep the national grid in its best condition to ensure an efficient, reliable, and effective network with minimal disruptions. In addition to these lines, NamPower’s asset base includes 156 transmission substations and 92 distribution substations with a total transformer capacity of 8,978 MVA, along with specialized HVdc and SVC devices.

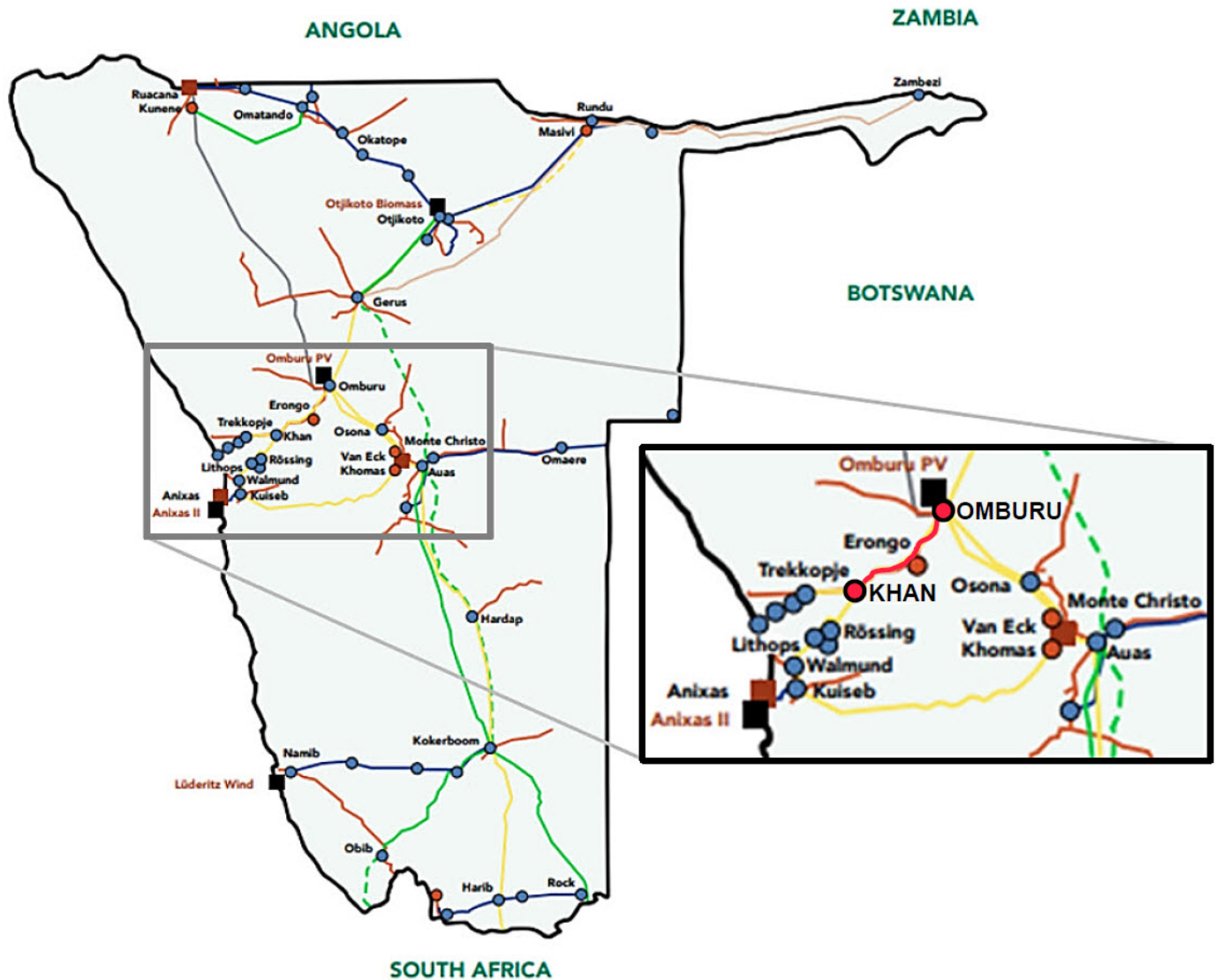


Fig. 1. NamPower transmission network (inset), showing a zoomed-in view of the 220 kV Omburu-Khan transmission line corridor [1].

Two 220 kV 113.6 km overhead lines (Line 1 and Line 2) connect the Omburu and Khan terminals. These are major transmission lines in NamPower's transmission network and pass over difficult, inaccessible terrain in the Kalahari Basin. Fig. 1 shows the NamPower transmission network and a zoomed-in view of the Omburu-Khan 1 line.

A. 220 kV Omburu-Khan Transmission Corridor

The Omburu-Khan transmission corridor (shown in Fig. 1) is critical in the NamPower electric power system. Sustained faults on either of these lines means loss of electric power

service to thousands of customers and critical mining industry loads around the Khan substation.

Fig. 2 shows the one-line diagram of the 220 kV Omburu-Khan transmission lines. Four bus reactors, a filter bank, and a static VAR compensator are at the 330/220/66 kV Omburu substation on the 220 kV bus. A 220 kV filter bank is at the 220/66 kV Khan substation. The 220 kV buses at Omburu and Khan substations are configured as a double-bus (not shown in Fig. 2) single-breaker scheme. Terminal equipment is listed in Table I, and line data are listed in Table II.

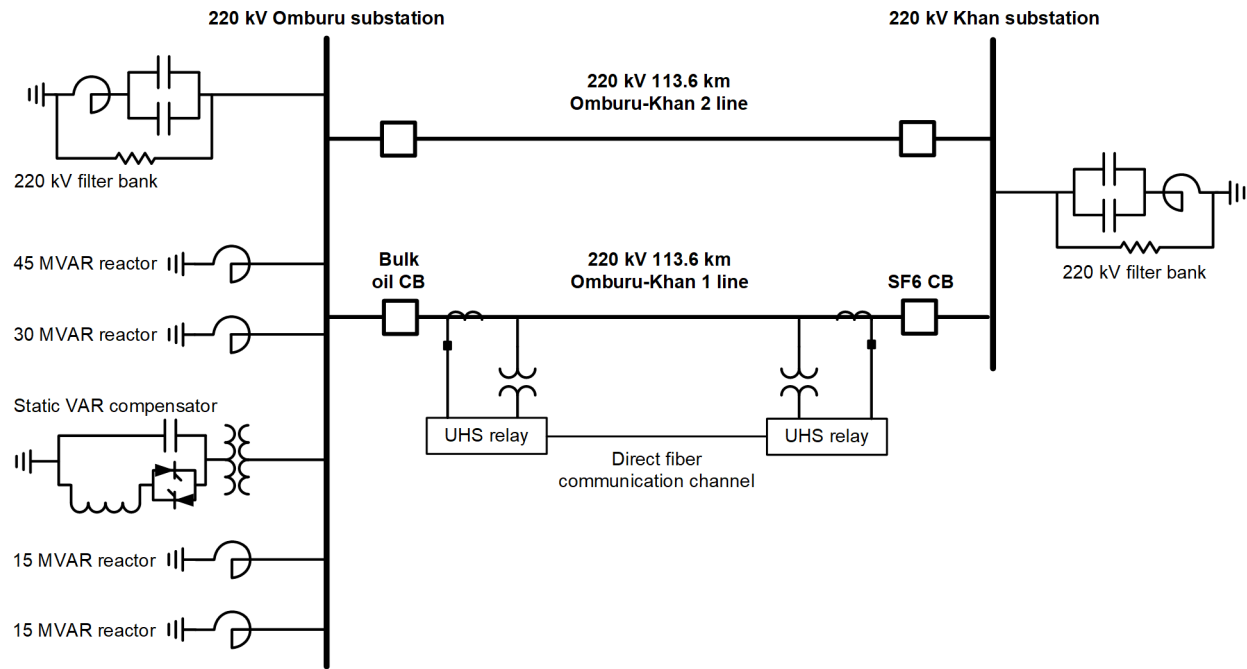


Fig. 2. Omburu-Khan 220 kV transmission corridor and substation buses.

TABLE I
TERMINAL EQUIPMENT

Equipment	Omburu	Khan
Line-to-Line Voltage	220 kV	220 kV
220 kV Outgoing Lines From Terminal	5	5
Current Transformer	Ratio: 800/1 A Class: TPS $I_m \leq 150$ mA $RCT \leq 3.2 \Omega$	Ratio: 800/1 A Class: TPS $I_m \leq 150$ mA $RCT \leq 3.2 \Omega$
Line coupling-capacitor voltage transformers (CCVT)	Y-Connected Ratio: 220 kV/110 V Class: 3P Burden: 100 VA	Y-Connected Ratio: 220 kV/110 V Class: 3P Burden: 100 VA
Circuit Breaker	Type: Bulk Oil Short Circuit Breaking Current: 30.3 kA for 3 s	Type: SF6 Short Circuit Breaking Current: 40 kA for 3 s

TABLE II
LINE DATA

Parameter	Value
Source Impedance at Omburu (ZSO)	36.97 Ω
Source Impedance at Khan (ZSK)	49.95 Ω
Positive-Sequence Line Impedance (Primary)	46.925 $\Omega \angle 77.78^\circ$
Zero-Sequence Line Impedance (Primary)	164.575 $\Omega \quad 75.41^\circ$
Line Length	113.6 km
Traveling-Wave Line Propagation Time (TWLPT)	386.66 μ s
Line Voltage	220 kV
CCVT Rating	220 kV/110 V Line-to-Line
CTR at Khan	800:1 A
CTR at Omburu	800:1 A

B. Line Protection on the Omburu-Khan 1 Line

Per the NamPower line protection standards, existing line protection on the Omburu-Khan 1 line uses phasor-based line current differential (87L) and step distance (21) protection, in conjunction with a permissive overreaching transfer trip (POTT) scheme. Fault locating is based on the single-ended impedance-based method.

The 87L scheme uses phase, negative-sequence, and ground elements. The differential relays are connected to each other using the direct fiber-optic communication channel. The phase current differential pickup is set to 1.2 pu (with or without line-charging-current compensation), and negative sequence and ground differential protection pickup levels are set between 0.1 and 0.15 pu. The distance protection practice at NamPower involves configuring four distance zones with Mho elements for phase faults and quadrilateral elements for ground faults. The POTT scheme uses the overreaching distance elements. The Zone 1 distance reach is set at 80 percent of the line impedance and is set to trip instantaneously. The Zone 2 reach is set to 120 percent of the line impedance, reaching beyond the remote bus and is set with a delay of 400 ms. Zone 3 is set as reverse, with the reach set to 45 percent of the line impedance; it is used for blocking and weak infeed schemes. Zone 4 is set to the same reach as Zone 2, but with a much longer operating time between 1 and 3 s. For accelerated tripping, in addition to the 87L scheme, NamPower uses the POTT scheme over the power line carrier (PLC) or optical ground wire (OPGW) fiber-optic channel. The direct transfer trip (DTT) scheme is also used to send a direct trip to the remote end in case of local breaker failure (BF). The weak infeed scheme is also implemented on radial lines or lines with weak terminals. All Zone 1 faults initiate autoreclosing; Zone 2 elements can only initiate autoreclosing if a permissive trip signal is received from the remote end. Zone 4 trips result in a lockout of the autoreclosing function. Negative- and zero-sequence-based directional overcurrent elements are used as backup protection to detect phase and ground faults.

The line has CCVTs at each end of the line. In general, phasor-based distance elements applied with CCVTs are prone to overreaching and face challenges in accuracy of operation [2]. The presence of voltage and power quality improvement equipment, like bus reactors, static VAR compensators, and filter banks at either end of the line challenge the operation of phasor-based distance protection elements [3]. The single-end impedance-based fault locating method included in the existing line protection faced the challenge to accurately locate faults on this line. NamPower wanted to improve fault-clearing times and the accuracy of locating faults, so when they learned of the new technology available with UHS relays, they decided to evaluate these relays and install a pair of UHS relays to monitor the Omburu-Khan 1 transmission line.

III. FIELD EXPERIENCE WITH UHS PROTECTION AND TRAVELING-WAVE FAULT LOCATING

UHS relays [4] include the TW-based differential (TW87) scheme, the TW-based directional (TW32) element, the incremental-quantity-based distance (TD21) element, and the incremental-quantity-based directional (TD32) element. UHS relays include TWFL methods to locate faults with a high level of accuracy. The ability of UHS relays to provide transient recording at a 1 MHz sampling rate and 18-bit resolution allows analysis of high-frequency power system events, including breaker reignition and post-fault arcing. These capabilities are unavailable in existing conventional microprocessor-based line protective relays.

On February 4, 2020, a C-phase-to-ground fault was recorded by the UHS relays monitoring the Omburu-Khan 1 line, as shown in Fig. 3 for the Omburu terminal and Fig. 4 for the Khan terminal. In Fig. 3 and Fig. 4, TD21G (incremental-quantity-based ground distance element) and TW87 (TW-based differential scheme) are digital output signals of the UHS relays. Z1T is the underreaching Zone 1 distance element digital output of the phasor-based relay on the line. This was the first fault on the line following the installation of the UHS relays. For the analysis of this fault, transient records were retrieved from the UHS relays at both terminals. In this section, we use the transient records captured by the UHS relays at the Omburu and Khan terminal to relate the fundamentals of the UHS protection and TW fault locating method with their performance in the field.

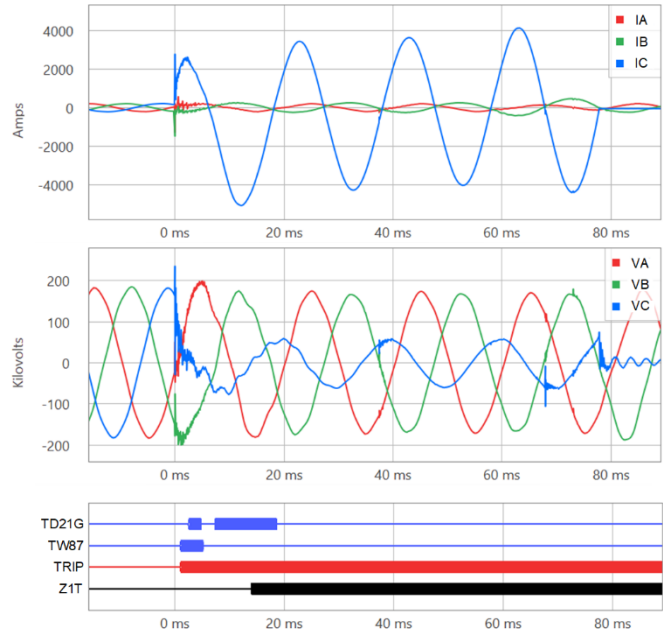


Fig. 3. Transient record oscillography and performance of UHS relay and phasor-based distance protection (Z1T) at the Omburu terminal.

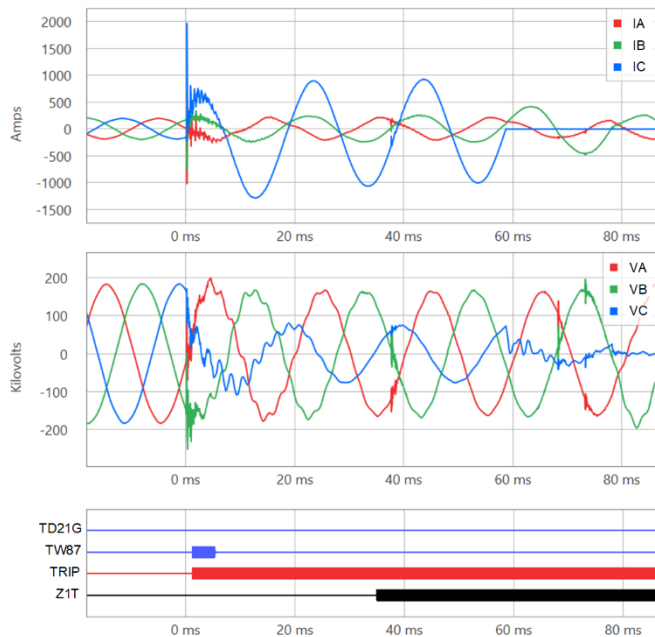


Fig. 4. Transient record oscillography and performance of UHS relay and phasor-based distance protection (Z1T) at the Khan terminal.

A. Transient Recording

The UHS relay provides transient recording functionality with two types of records:

- Ultra-high-resolution record containing voltages and currents (megahertz record [MHR], 1 MHz sampling rate).
- High-resolution record containing voltages and currents, derived protection quantities, and all digital bits (time-domain record [TDR], 10 kHz sampling rate).

Both types of records are stored in IEEE C37.111-2013 COMTRADE format. As per this format, both the MHR and TDR IEEE COMTRADE records are comprised of three files: configuration (CFG) file, data (DAT) file, and header (HDR) file. The three-letter abbreviations serve as the file extension type. The CFG file describes the content of the DAT file, the DAT file contains the values for each input channel for each sample in the record, and the HDR file contains relay settings and event-related analog quantities (such as pre-fault and fault voltages and currents, fault type and location, etc.), which are helpful when analyzing power system events and relay operations [4] [9].

Event analysis software [10] enables the user to open the MHR IEEE COMTRADE records and plot the voltage and current signals, obtain phase TWs, obtain modal TWs (zero, alpha, and beta Clarke components) for manual analysis, and apply time cursors that replicate the interpolation method used by the UHS relays to obtain the TW arrival time with submicrosecond accuracy [8], as shown in Section IV of this paper. The time stamp of the initial TW at each terminal may be obtained by opening the corresponding MHR IEEE COMTRADE records in the event analysis software, plotting the appropriate modal TW signal according to the fault type, and sliding the time cursor to line up with the peak of the initial TW. It is important to note that this time stamp does not include compensation for the TW current transformer (CT) cable delay. The event analysis software also provides the ability to plot and analyze Bewley diagrams.

B. TW-Based Line Protection: TW87 and TW32

The UHS protective relays in the pilot installation included a TW-based directional (TW32) element and a TW-based differential (TW87) scheme. References [5] and [6] discuss TW-based protection principles and their field performance in detail. The nature of current and voltage TWs for different fault conditions is summarized in this section and aids in analyzing the performance of TW87 scheme and TW32 element observed during the fault.

1) TW87 Scheme

a) TW87 Scheme Fundamentals

For an internal fault on the line, the first current TWs detected at the local and remote line terminals have the same polarity and are separated by less than the TWLPT. TWLPT is the one-way end-to-end travel time of the TW along the transmission line. TWLPT is a configuration setting required by the UHS relays. The accuracy of the TWLPT setting is critical for the security of the TW87 protection scheme and for the accuracy of the TWFL methods. TWLPT is measured by using the transient record captured during a line energization test, as recommended in [7].

When the fault is external to the line, the first current TWs detected by the local and remote line terminals have opposite polarities and are separated by the TWLPT. This is the fundamental principle of the TW87 scheme. The TW87 scheme requires that the UHS relays at each line terminal exchange measurements of the local voltage and current signals sampled at 1 MHz using the dedicated fiber-optic channel. With the dedicated fiber-optic channel connected, the relays are time-synchronized and do not rely on an external time source. Additional implementation details of the TW87 scheme in UHS relays are available in [4].

b) TW87 Scheme Performance

Line energization tests were performed during commissioning, and the TWLPT for the 220 kV Omburu-Khan 1 line was measured to be 386.66 μs . In this application of UHS relays, the relay-to-relay communication was established via a dedicated point-to-point fiber-optic channel. Reference [4] describes the relevance of TWLPT and direct fiber communications to the TW87 scheme. The TW87 scheme compares timing, polarities, and magnitudes of current TWs at both line terminals. The TW87 scheme asserted in less than 1.1 ms at the Omburu terminal and in less than 1.3 ms at the Khan terminal (as shown in Fig. 5). The first TWs arriving to the two terminals are of the same polarity and have an arrival time difference of 239.422 μs (as observed in Fig. 12), which is less than the TWLPT. This is the signature of an internal fault.

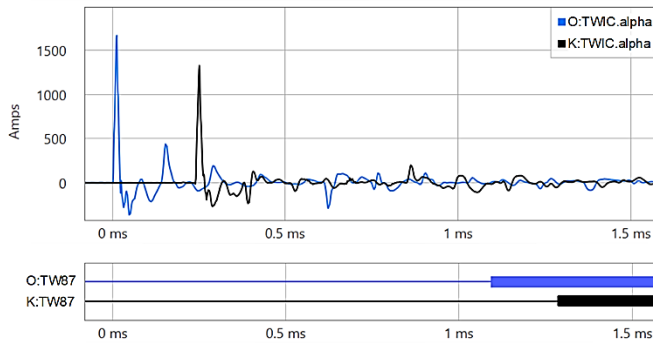


Fig. 5. C-phase alpha-mode current TWs and operation of the TW87 scheme at the Omburu (O) and Khan (K) terminals.

2) TW32 Element

a) TW32 Fundamentals

The polarities of the first voltage and current TWs that arrive at one terminal after a fault occurs indicate the direction of the fault. When the fault is in the forward direction, the voltage TW and current TW have opposite polarities; for a reverse fault, the voltage TW and current TW have the same polarity. This fundamental principle forms the basis of TW32 element. The TW32 element in the UHS relay is used only for fast keying of the POTT scheme and is not intended for direct tripping of circuit breakers. Additional implementation details of the TW32 element and POTT scheme in the UHS relay are available in [4].

b) TW32 Element Performance

Theoretically, a wide-bandwidth (high-fidelity) voltage transformer is ideal to measure voltage TWs. However, in most cases, the UHS relays can measure the first voltage TW even with a CCVT because of interwinding capacitance across the step-down transformer and the interturn capacitance across the CCVT tuning reactor [7]. This voltage TW measurement is not accurate in terms of voltage TW magnitude, but it is accurate in terms of the arrival time and polarity, which is sufficient for the TW32 element. With CCVTs at either end of the line, we observed that the TW32 element declared the fault to be forward (TW32F asserted) in less than 100 μs at Omburu and Khan terminals. Remember that the opposite polarities of TW currents and TW voltages indicate a forward event from both terminals, as highlighted in Fig. 6 and Fig. 7.

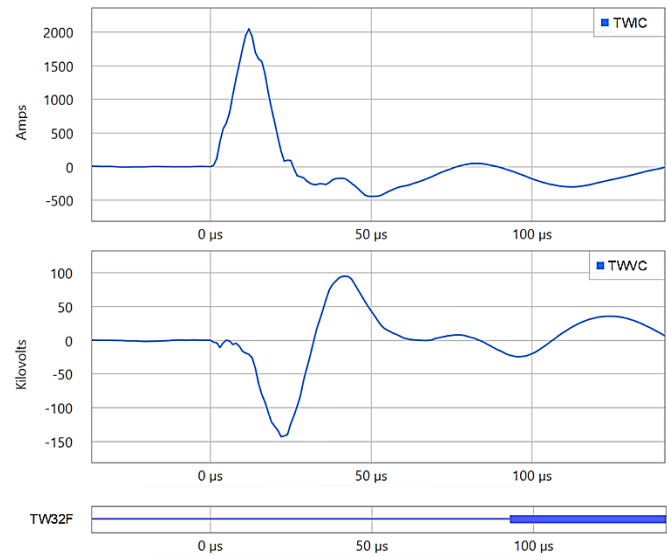


Fig. 6. C-phase current and voltage TWs and operation of the TW32 element at the Omburu terminal.

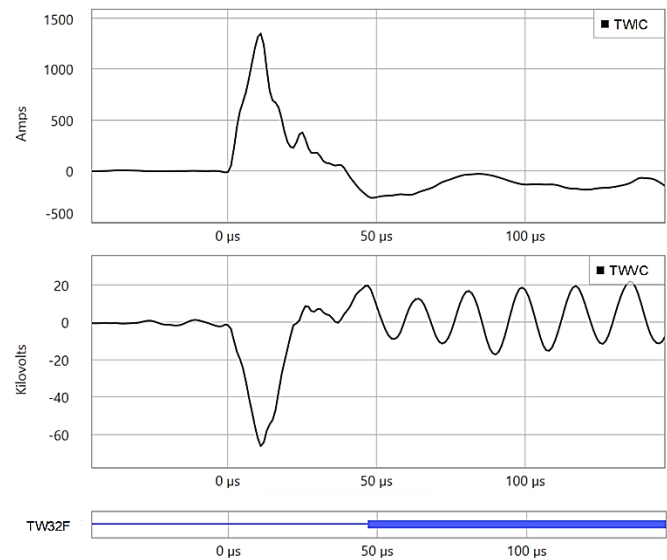


Fig. 7. C-phase current and voltage TWs and operation of the TW32 element at the Khan terminal.

Although the POTT scheme was not enabled at the time of this fault, NamPower was interested in the performance of the TW32 element as part of their consideration for enabling the POTT scheme with keying of the permissive trip signal from the TW32 element in the future.

C. Incremental-Quantity-Based Protection: TD21 and TD32

The UHS protective relays included protection elements that use voltage and current incremental quantities, which are the differences between a present instantaneous sample and a one-cycle-old sample. The incremental quantities contain the pure fault voltage and current information and exclude any pre-fault load information [2]. These signals are filtered with a low-pass filter and are used to realize the incremental-quantity-based directional (TD32) and distance (TD21) elements. The relay calculates incremental voltage and incremental replica currents for six measurement loops [4].

1) TD21 Element

a) TD21 Element Fundamentals

The TD21 element is a fast-underreaching Zone 1 distance element used for instantaneous tripping. This element calculates the incremental voltage change at the reach point (operating voltage) and compares it with the pre-fault voltage at the same reach point (restraint voltage). For an in-zone fault within the reach point, the calculated incremental voltage change at the reach point will be greater than the pre-fault reach point voltage. For a fault beyond the reach point (outside the zone of protection), the calculated incremental voltage change at the reach point will be less than the pre-fault reach point voltage [4].

b) TD21 Element Performance

For this C-phase-to-ground fault, the TD21 ground element (TD21G) asserted at Omburu. With the TD21G reach set at 70 percent and the fault located at 19 percent of the line (21.629 km/113.60 km) from Omburu, the fault is well within the Zone 1 element reach and operated in 2.59 ms (Fig. 8a and Fig. 8b). The TD21 element operated because the operating voltage was greater than the restraining voltage, as shown in Fig. 8b. From the Khan terminal, the fault located at 81 percent ($1 - 0.19$ pu) was beyond the 70 percent reach of the TD21G element; therefore, the TD21 restrained from operating, shown in Fig. 8c. Fig. 8c shows that the operating voltage was less than the restraining voltage at Khan.

Fig. 8a

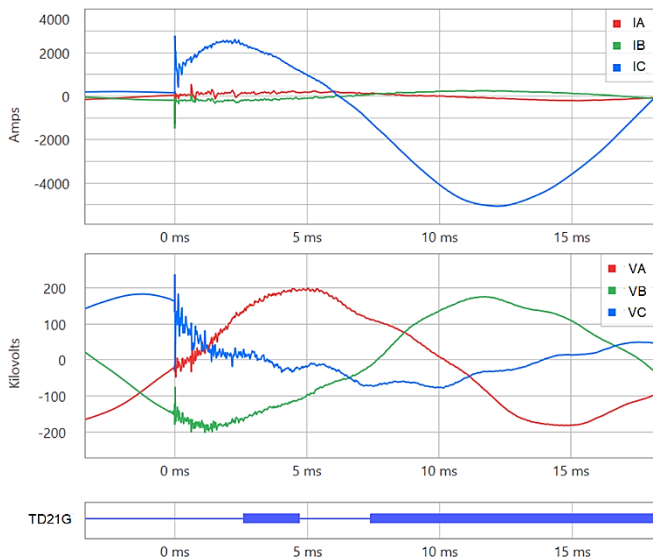


Fig. 8b

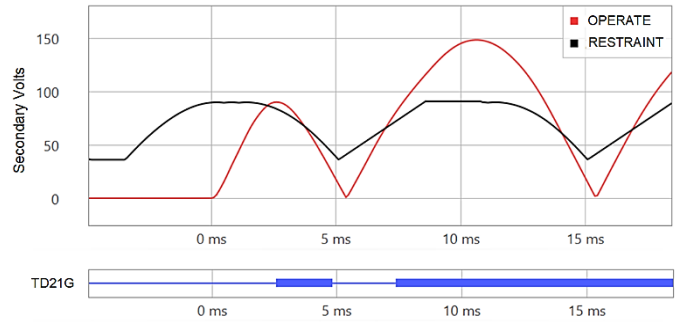


Fig. 8c

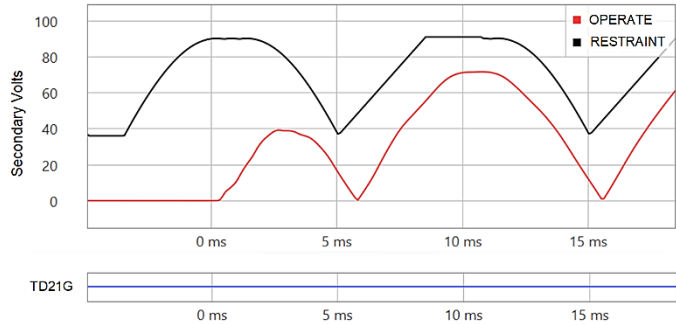


Fig. 8. (a) Current and voltage captured by the UHS relay at Omburu, (b) operate and restrain voltage profiles and operation of the TD21 ground (TD21G) element at Omburu, and (c) operate and restrain voltage profiles and TD21G element restraining at Khan.

2) TD32 POTT Scheme

a) TD32 Fundamentals

The TD32 element provides a fast, secure, and dependable directional indication. This element is used as part of a POTT scheme and is not intended for direct tripping of circuit breakers. The TD32 element calculates the operating torque as a product of sign-inverted incremental loop voltage and incremental replica loop current. It also calculates the forward and reverse restraining torques based on the incremental replica loop current and relay settings for the forward/reverse impedance thresholds. For a forward fault, the incremental loop voltage and incremental replica loop current have opposite polarities, which results in a positive torque. For a reverse fault, the incremental loop voltage and incremental replica loop current have the same polarity, which results in a negative torque. The calculated torques are integrated (accumulated), and the integrated operating torque is compared with the integrated restraining torques. The TD32 element declares forward if the integrated operating torque is positive and exceeds the integrated forward restraining torque. Reference [4] discusses the TD32 element in detail.

b) TD32 Element Performance

The incremental-quantity directional (TD32) element operated and detected the fault as forward (TD32F) in both relays. The TD32F digital logic asserted in 1.09 ms at Omburu (shown in Fig. 9a and Fig. 9b) and in 1.15 ms at Khan (shown in Fig. 10a and Fig. 10b). In Fig. 9a and Fig. 10a, the incremental-quantity replica loop current is opposite in polarity to the incremental-quantity loop voltage at the Omburu and Khan terminals, respectively. The incremental-quantity replica current for the C-phase-to-ground loop can be calculated using custom calculations in the event analysis software ($DIZCG = DIZC - DIZ0$) [4]. Fig. 9b and Fig. 10b show the operating torque, forward restraining torque, and reverse restraining torque for the respective terminals. They also show that the accumulated operating torque is positive and exceeds the accumulated forward restraining torque, resulting in the assertion of TD32F in both relays.

Fig. 9a

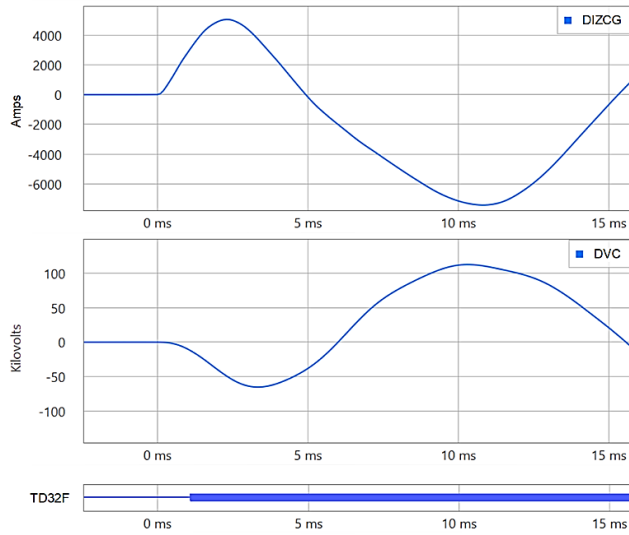


Fig. 9b

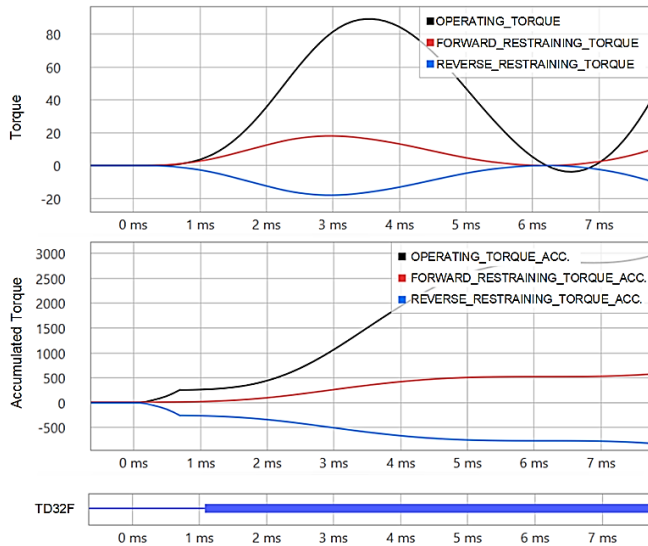


Fig. 9. a) Incremental-quantity replica loop current and incremental-quantity loop voltage captured by the UHS relay at Omburu and b) accumulated operating and restraining torques and operation of the TD32 element at Omburu.

Fig. 10a

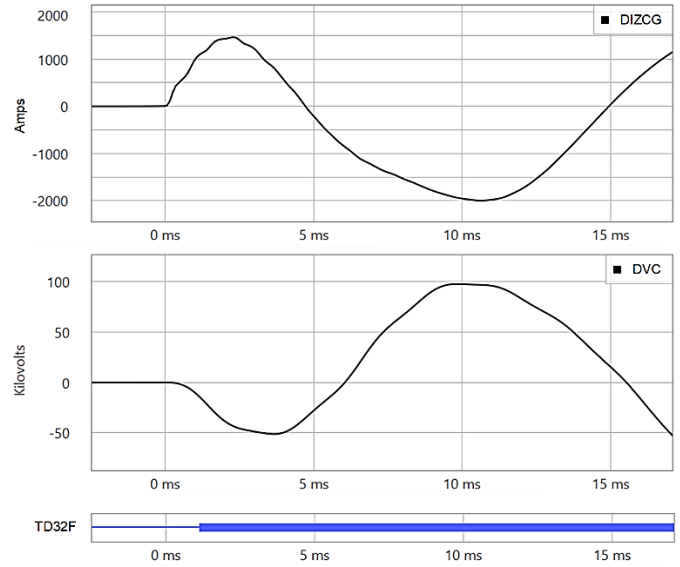


Fig. 10b

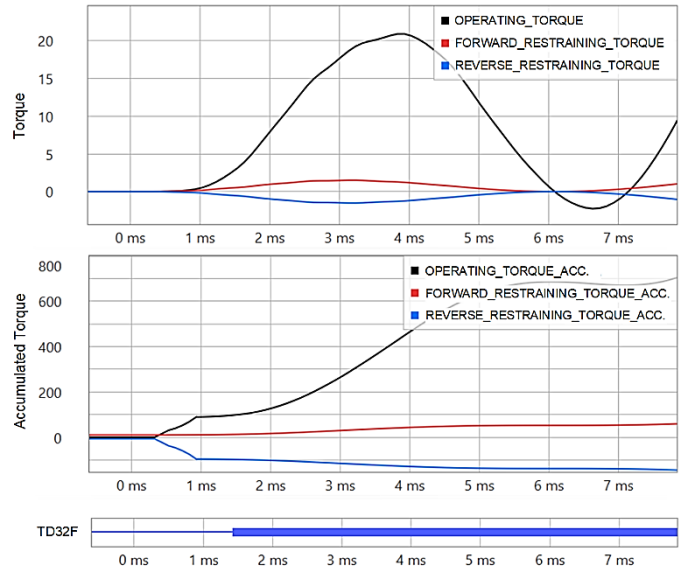


Fig. 10. a) Incremental-quantity replica loop current and voltage captured by the UHS relay at Khan and b) operating and restraining torques and operation of the TD32 element at Khan.

D. TW-Based Fault Locating

1) TWFL Fundamentals

Faults on transmission lines generate TWs that propagate from the location of the fault to the line terminals. The fault location can be calculated based on the TW arrival times, the line length (LL), and the TWLPT. TWFL is widely popular with transmission system operators, largely due to its field-proven track record with reported errors being within one tower span (300 m or 1,000 ft) on average, regardless of LL.

The UHS relays applied in this pilot application include the following methods:

- Single-ended traveling-wave-based fault-locating (SETWFL)
- Double-ended traveling-wave-based fault-locating (DETWFL)
- Single-ended impedance-based fault-locating (SEZFL)
- Double-ended impedance-based fault-locating (DEZFL)

The DETWFL method uses the arrival times for the initial TW at both terminals, along with the LL and the TWLPT, to calculate the fault location. In this application, a direct fiber-optic connection was available between the Omburu-Khan line terminals and was used for the DETWFL method. The general equation used to calculate DETWFL results is shown in (1). M is the calculated fault location, t_L is the arrival time of the initial TW at the local terminal, and t_R is the arrival time of the initial TW at the remote terminal.

$$M = \frac{LL}{2} \cdot \left(1 + \frac{t_L - t_R}{TWLPT} \right) \quad (1)$$

The UHS relays were also capable of compensating (1) by using (2) and the TW CT cable propagation time setting (TWCPT) in each relay to increase the accuracy of DETWFL by compensating for the time delay that is introduced by the cables between the CTs and the relay. The compensation is not needed if both relays use CT cables with the same propagation time (similar cable types with similar lengths). The fault locator adjusts for the associated time delay by backdating the initial TW time stamps at both terminals [9].

$$M = \frac{LL}{2} \cdot \left(1 + \frac{(t_L - t_R) - (TWCPT_L - TWCPT_R)}{TWLPT} \right) \quad (2)$$

In installations when relay-to-relay communications are unavailable, the arrival time of the initial TW at each terminal can be obtained by various means, as described in [9]. The UHS relays also provide a calculated fault location using the SETWFL method. This is particularly useful when the fiber-

optic channel used for relay-to-relay communications (either a dedicated point-to-point direct fiber-optic channel or IEEE C37.94 multiplexed communications with submicrosecond time-synchronized relays) is unavailable for a given application, the fiber-optic channel is temporarily out of service, or a single relay is installed on a radial line.

2) DETWFL Performance

The direct fiber-optic channel is used to exchange 1 MHz sampled voltages and currents between the UHS relays at Omburu and Khan. Each UHS relay time-stamps the arrival of the first TW associated with the local currents and received remote currents. With the arrival time of the initial TW at the local and remote terminals known, each UHS relay automatically calculates the fault location using the DETWFL method by applying the TW arrival times, along with relay settings for LL and TWLPT, in (1).

The Bewley diagram in Fig. 11 shows the C-phase TW alpha-mode currents from the Omburu and Khan terminals. The Bewley diagram provides a visualization of the TWs for the fault and allows for verification of the DETWFL result.

The UHS relays located the fault at 21.629 km from Omburu and 91.971 km from Khan. Fig. 12 displays the C-phase alpha-mode current TWs captured by the UHS relays at the Omburu and Khan terminals and shows the relative arrival time difference of 239.422 μ s between the first TWs at each terminal. It also shows that the initial TWs that arrived at each terminal have the same polarity (positive) and are separated by less than the TWLPT for this line (386.66 μ s).

When time-synchronized MHR IEEE COMTRADE records from the UHS relays at each terminal of the line are opened in a single session of the event analysis software, the event analysis software allows the user to plot the Bewley diagram and automatically align the local and remote TW peaks to display the fault location relative to either terminal of the line (see Fig. 11).

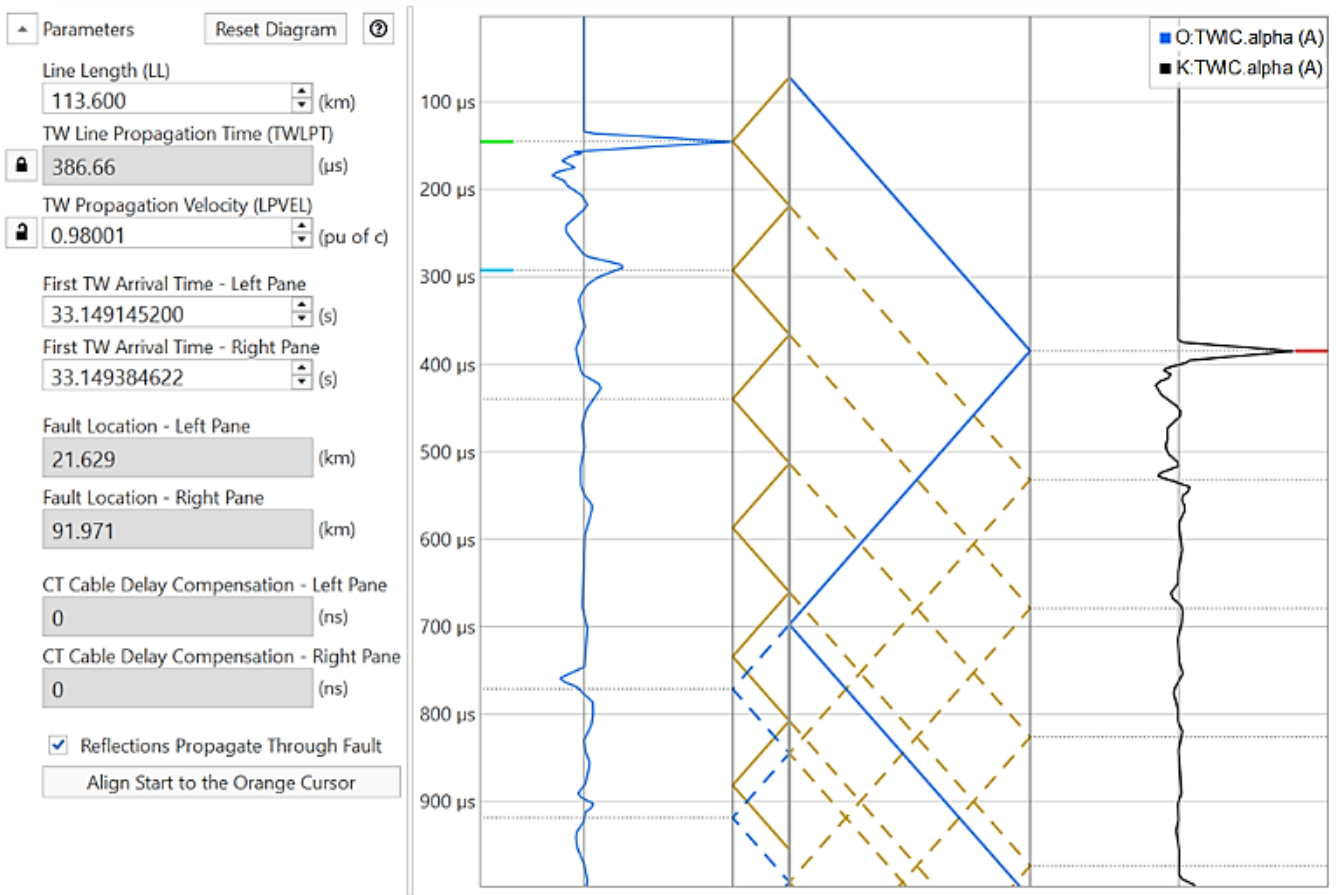


Fig. 11. Bewley diagram showing C-phase alpha-mode current TWs for the Omburu (O) and Khan (K) terminals.

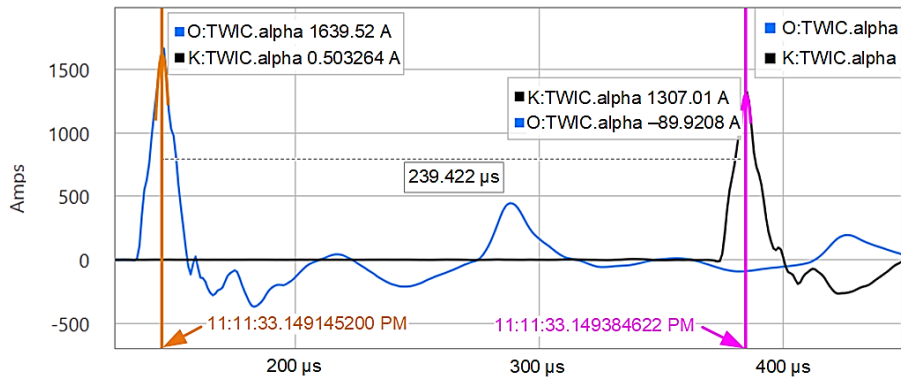


Fig. 12. C-phase alpha-mode current TWs captured by the UHS relays at Omburu (O) and Khan (K), showing the difference in arrival times of the initial TW at each terminal.

The time stamps for the initial TW that arrived at each terminal can also be confirmed from the fault location information in the HDR file of the MHR or TDR IEEE COMTRADE records from either terminal. Fig. 13 shows the fault location information in the HDR file from the UHS relay at Omburu.

```
[Fault_Location]
SE_TW_Location1,"21.047 (km) "
SE_TW_Location2,"$$$$$$ (km) "
SE_TW_Location3,"$$$$$$ (km) "
SE_TW_Location4,"$$$$$$ (km) "
DE_TW_Location,"21.629 (km) "
SE_Z-Based_Location,"24.638 (km) "
DE_Z-Based_Location,"18.768 (km) "
First_TW_Time_Local,"2020/02/04,06:11:33.149145200"
First_TW_Time_Remote,"2020/02/04,06:11:33.149384622"
```

Fig. 13. Fault location information in the Omburu UHS relay HDR file.

The fields in Fig. 13 are described as follows:

- SE_TW_Location ($n = 1, 2, 3, 4$) are the fault locations from the SETWFL method.
- DE_TW_Location is the fault location from the DETWFL method.
- SE_Z-Based_Location is the fault location from the SEZFL method.
- DE_Z-Based_Location is the fault location from the DEZFL method.
- First_TW_Time_Local is the time stamp of the first local TW.
- First_TW_Time_Remote is the time stamp of the first remote TW.

The information in Fig. 13 confirms that the relay automatically calculated the fault location using the DETWFL method (DE_TW_Location is 21.629 km). This result can also be verified manually by using the time difference in arrival times of the initial TW at each terminal in (1). Since the UHS relays at the Omburu and Khan terminals have identical cables with similar lengths from the CTs to the relays, the TWCPT compensation is unnecessary. The time difference can be obtained by either plotting the analog TW signals in the event analysis software (as shown in Fig. 12) or by using the First_TW_Time_Local and First_TW_Time_Remote values from the HDR file (as shown in Fig. 13). The fault location from Omburu and Khan, is calculated using (3) and (4), respectively:

$$M_{\text{Omburu}} = \frac{113.6 \text{ km}}{2} \cdot \left(1 + \frac{-239.422 \mu\text{s}}{386.66 \mu\text{s}} \right) = 21.629 \text{ km} \quad (3)$$

$$M_{\text{Khan}} = \frac{113.6 \text{ km}}{2} \cdot \left(1 + \frac{239.422 \mu\text{s}}{386.66 \mu\text{s}} \right) = 91.971 \text{ km} \quad (4)$$

During analysis, it was discovered that the settings in the UHS relays for the positive-sequence impedance of the Omburu-Khan 1 line are different than those used in the existing phasor-based relays; therefore, incorrect values were assumed to be used in the UHS relays and led to errors in the fault location results from the impedance-based methods. To confirm, the event records were played back on an identical pair of UHS relays in a bench test setup. Based on pre-fault data, the positive-sequence line impedance was determined to be $47.763 \Omega \angle 77.121^\circ$, which is consistent with the settings used in the existing phasor-based relays. Correcting the setting of the relays on the test bench with this value of positive-sequence line impedance improved the impedance-based fault location results. The corrected DEZFL result was 20.117 km and 103.252 km, and the corrected SEZFL result was 21.636 km and 93.484 km for the relays simulating the Omburu and Khan terminals, respectively. This shows that accurate line parameter settings are necessary for obtaining accurate fault location results by using impedance-based methods. Similarly, accurate LL and TWLPT settings are necessary for obtaining accurate fault location results by using TW-based methods.

IV. FAULT-CLEARING TIME AND CRITICAL CLEARING TIME

A. Fault-Clearing Time

Fault-clearing time (FCT) is well-defined in Section III (Part A) of [11]. At Omburu, the existing phasor-based underreaching Zone 1 distance element (Z1T in Fig. 3) operated in 13.87 ms for this fault and issued a C-phase single-pole trip to the breaker. The bulk oil circuit breaker at Omburu took 63 ms to clear the fault, for a total FCT of 76.87 ms (see Fig. 3).

At Khan, the existing phasor-based underreaching Zone 1 distance element (Z1T in Fig. 4) operated in 35 ms, and the SF6 circuit breaker opened in another 23.7 ms. The total FCT was 58.7 ms (see Fig. 4). In comparison to the operating time of the phasor-based relays, the UHS relays operated almost 13 ms faster at Omburu and nearly 34 ms faster at Khan.

The UHS relays were not wired to trip the circuit breaker at the time of the fault; however, at the time of writing this paper, the UHS relays are wired for tripping (fault-clearing) to improve FCT over the existing phasor-based protective relays, as shown in Table III. It is important to note that the Khan terminal has a fast SF6 circuit breaker.

TABLE III
FCT COMPARISON

Equipment	Omburu	Khan
Circuit Breaker	Type: Bulk Oil Short Circuit Breaking Current: 30.3 kA for 3 s	Type: SF6 Short Circuit Breaking Current: 40 kA for 3 s
Existing Phasor-Based Relay Operate Time (ms)	13.87	35
Breaker Trip Time (ms)	63	23.7
FCT (ms)	76.87	58.7
UHS Relay Operate Time (ms)	1.092	1.05
UHS FCT (ms)	64.092	24.75
FCT Difference (ms)	12.778*	33.95*
Percentage Reduction	16.6%	57.8%

*Note: FCT reduction time expected to be 20 ms (1 cycle at 50 Hz) as is typically observed from other UHS relay installations [12].

B. Critical Clearing Time

First swing transient stability is the ability of the electric power system to remain in electromechanical equilibrium during abnormal and large disturbance operating conditions [14]. Critical clearing time (CCT) is determined from a transient stability study, by solving the nonlinear differential swing equation for rotor angle δ as a function of time (t) for the unit under study. CCT is the maximum allowable time to clear a short circuit fault to ensure the entire system remains stable, preventing loss of synchronism.

Modern electric power systems typically have reduced transmission capacity margins and are operating nearer to their stability limits. This is due to new additional generation capacity without increasing transmission capacity driven by deregulation, economic priorities, reducing transmission investment, or the difficulty of securing the right of way. Short FCTs reduce stress in the power system and improve power quality and power transient stability. Short fault duration allows sensitive equipment to ride through the disturbance and stay connected to the power system. An improved FCT reduces the possibility of a loss of synchronism during a BF condition, by increasing the margin between the BF clearing time and the CCT.

Section III (Part B) of [15] explains the swing equation for a lossless two-machine system, steady-state stability limit at power (or rotor) angle δ equals 90 degrees and uses the equal-area criteria method to show the power transfer capability in unstable and stable power systems. Discussion regarding first swing transient stability and electric power system electromechanical equilibrium theory is beyond the scope of this paper; hence, readers are encouraged to reference classical electric power system analysis textbooks [14] [16] [17].

Fig. 14 shows the power-angle and time-angle swing curves using equal-area criteria method. Under normal (pre-fault) operating conditions, the mechanical power (P_M) supplied to the generator equals its electrical power output (P_E), and the rotor angle is δ_0 ($P_E = P_M = P_{MAX} \cdot \sin \delta_0$). P_{MAX} is the maximum electric power that can be transferred on the line. This is Point 0 in Fig. 14a. Fig. 14a also shows the three P_E power-angle curves that represent the power transfer during pre-fault, fault, and post-fault conditions. Transferred power is shown, as follows.

$$\text{Prior to the fault: } P_E = P_{MAX} \cdot \sin \delta_0$$

$$\text{During the fault: } P_E = r_1 \cdot P_{MAX} \cdot \sin \delta$$

$$\text{After the fault: } P_E = r_2 \cdot P_{MAX} \cdot \sin \delta$$

where:

r_1 is the ratio of maximum electric power during the fault to P_{MAX} .

r_2 is the ratio of maximum electric power post fault to P_{MAX} .

When the fault occurs, the system transitions to the fault power-angle curve (Point 1), and since P_M is greater than P_E , the generator rotor accelerates and δ increases. When the fault is cleared in FCT (t_c) at Point 2, δ equals δ_c , the system transitions again through Point 3 to the post-fault curve (Point 4) as the fault is removed, and the system has lost the transmission line. Area A_1 (Points 0, 1, 2 and 3) represents the kinetic energy of the rotor when P_M is greater than P_E (the acceleration region). At Point 4, the post-fault system, P_E is greater than P_M , and the generator decelerates, but δ continues increasing because the generator speed is greater than the synchronous speed. The angle δ increases up to the value δ_{MAX}^U

for Area A_2 (Points 3, 4 and 5), which represents the kinetic energy drawn from the generator rotor. Once the rotor angle increases beyond the maximum, P_M is greater than P_E , and the rotor accelerates again. Fig. 14a shows an unstable system because Area A_1 is greater than Area A_2 . At Point 5, P_M is greater than P_E , the generator begins to accelerate again, the rotor angle continues to increase, and the unit slips a pole once the rotor angle δ becomes greater than 180 degrees. Hence, the maximum angle post-fault that causes P_E to equal P_M (Point 5) is denoted as δ_{MAX}^U for this unstable condition.

Fig. 14b is similar to Fig. 14a, but in this case, t_c is a shorter duration; hence, it is a smaller δ_c and Area A_1 equals Area A_2 at Point 5 (note that δ_X is less than δ_{MAX}), so the system is stable. Furthermore, Fig. 14c shows a special condition between Fig. 14a and Fig. 14b that defines CCT (t_{cr}), which is the time at the critical clearing angle δ_{cr} that results in Area A_1 equaling Area A_2 . This is the boundary condition for stability. The maximum angle post-fault that causes P_E to equal P_M (Point 5) is denoted as δ_{MAX}^S for this boundary condition. Note that when δ_c is greater than δ_{cr} , Area A_1 is greater than Area A_2 , and the power system becomes unstable, as shown in Fig. 14a.

Fig. 14a

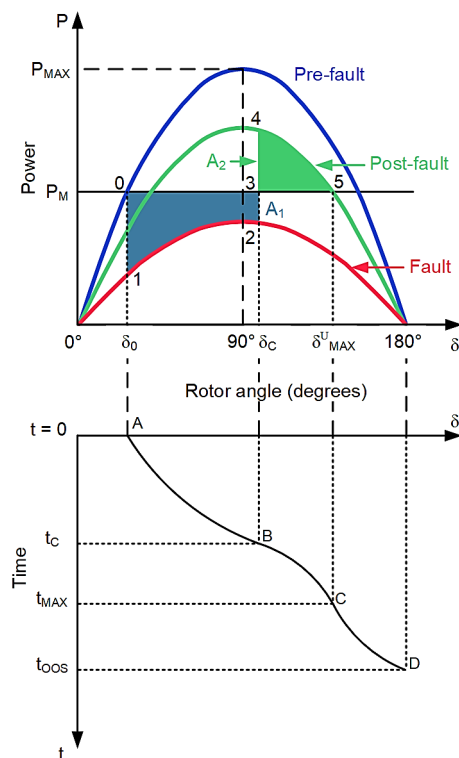


Fig. 14b

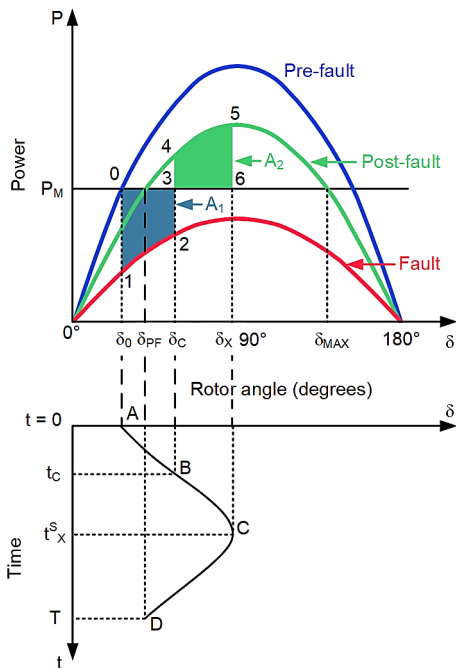


Fig. 14c

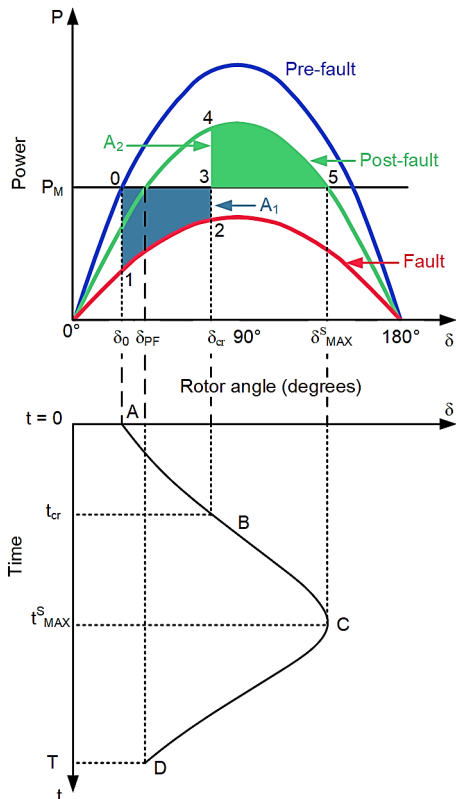


Fig. 14. Power-angle and time-angle swing curves using equal-area criteria method for (a) an unstable system with δ_{MAX}^U , (b) a stable system with $\delta_X < \delta_{MAX}$, and (c) critical stable system $\delta_C = \delta_{cr}$ and $\delta_X = \delta_{MAX}^S$.

After evaluating the equal Areas A_1 and A_2 in Fig. 14c, during the fault, note that δ_{cr} from Equation 16.73 in [14] is determined as the solution from (5).

$$\cos \delta_{cr} = \frac{\left(\frac{P_M}{P_{MAX}} \right) (\delta_{MAX} - \delta_0) + r_2 \cos \delta_{MAX} - r_1 \cos \delta_0}{r_2 - r_1} \quad (5)$$

However, CCT cannot be expressed in a single equation and requires obtaining the time-angle swing curve for the generator. Generator rotor angle vs. time swing curves, as shown graphically in bottom half of Fig. 14a, Fig. 14b, and Fig. 14c, are calculated using a computer numerical method, such as the fourth order Runge-Kutta method [14] [17]. These calculations can be used to study large interconnected systems with numerous generators and motors.

For the Omburu-Khan 1 line, the CCT is 240 ms with all lines in service. NamPower's standard BF time delay is 120 ms. Based on Table III, phasor-based relay operate times are 13.87 ms for the Omburu terminal and 35 ms for the Khan terminal. The BF time delay added to these relay operate times leaves 106 ms at Omburu and 85 ms Khan for the remainder of the BF clearing time (BFCT) and CCT margin time with all lines in service. FCT and BFCT can be improved with UHS relays, as observed for this C-phase-to-ground fault. In this application, the slowest operating time of the TD32 POTT scheme and the slowest breaker operating time is a good reference to determine the BF delay; with this approach, we can ensure that coordination is maintained for all faults in the line. For this application that uses UHS relays, a conservative BF delay of six cycles provides a good coordination margin between the BFCT and the FCT for the Omburu-Khan 1 line that results in an increase in the CCT margin. Fig. 15 illustrates how UHS protection increases the CCT margin.

As noted in 17.1.1 of [17], a further 0.5 to 1 cycle reduction (10 to 20 ms at 50 Hz and 8.33 to 16.67 ms at 60 Hz) in the FCT can be achieved when the industry replaces two-cycle circuit breakers with one-cycle circuit breakers.

To improve transient system stability and power quality, protection and studies engineers may consider applying UHS relays to protect transmission lines. Furthermore, faster circuit breakers can help reduce the FCT. The use of these technologies could be the preferred solution and more economically feasible than the design and construction of new parallel transmission lines or the addition of series compensation to an existing transmission line.

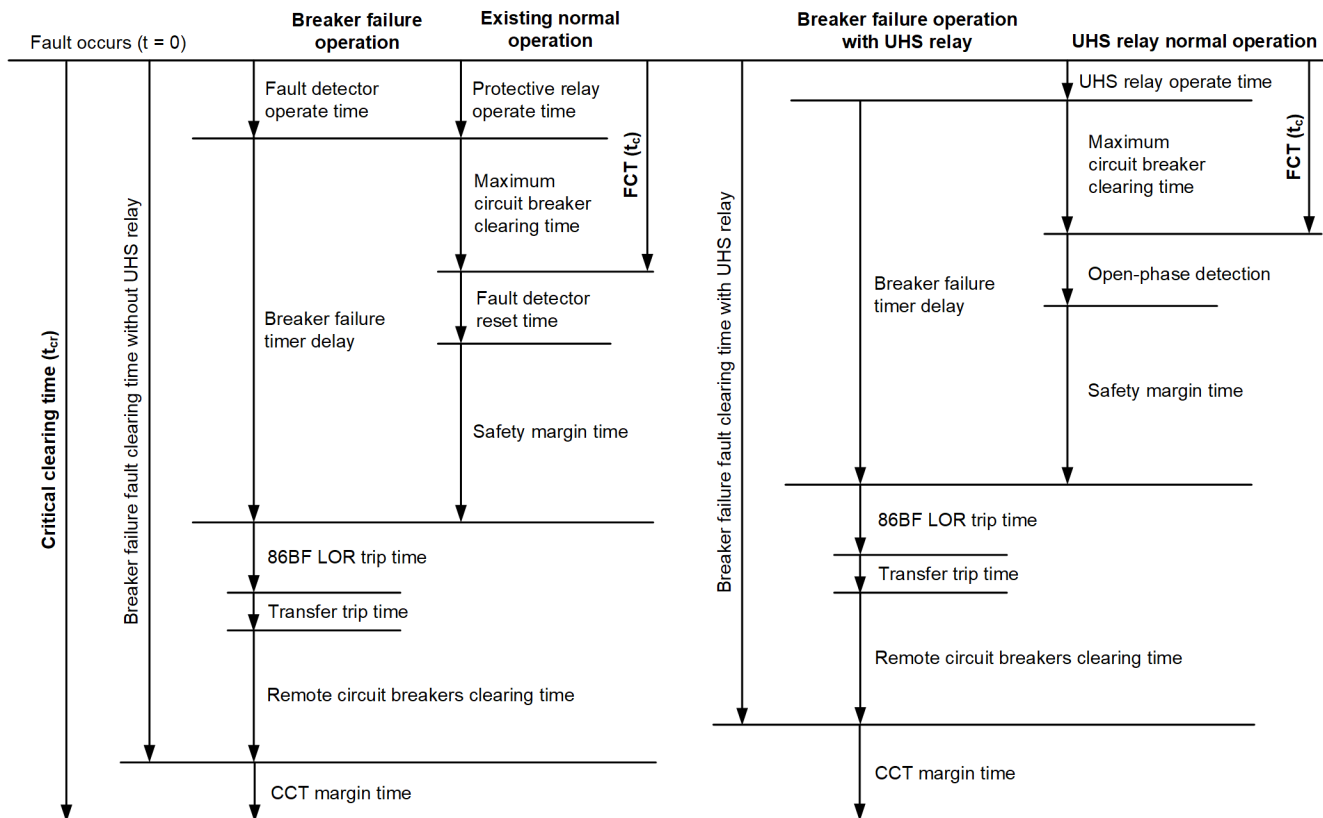


Fig. 15. Simplified CCT, BFCT, FCT, and CCT margin time chart for both phasor-based [18] and UHS relays.

V. POST-FAULT ARCING AND BREAKER REIGNITION OBSERVED IN 1 MHz TRANSIENT RECORDS

While reviewing the fault current profile of the C-phase from both terminals and comparing them, we observed that there are two additional instances when TWs were launched before the fault was cleared (see Fig. 16).

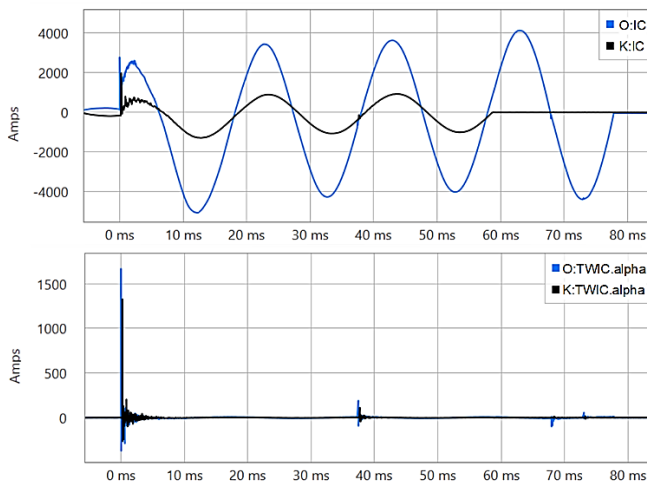


Fig. 16. Measured C-phase currents and alpha-mode TWs observed by the UHS relays at Omburu (O) and Khan (K), showing additional disturbances following the fault initiation.

The first instance occurred 37.5 ms after the fault initiated and was caused by a second arcing fault that occurred at the same fault location, launching TWs that were received at Omburu and Khan. Multiple reflections between the fault

location and each line terminal can be seen for this instance. A zoomed-in view of the C-phase current and C-phase alpha-mode current TWs is shown in Fig. 17. This disturbance occurred 2 cycles before the Omburu breaker opened and 1 cycle before the Khan breaker opened, and it launched TWs that arrived at the Omburu terminal 237.398 μ s before arriving at the Khan terminal. Additionally, both of the initial TWs that arrived at the line terminals have positive polarity. These observations confirm that the disturbance is internal to the line and confirm the recurrence of a fault that originated at or close to the same location as the initial fault.

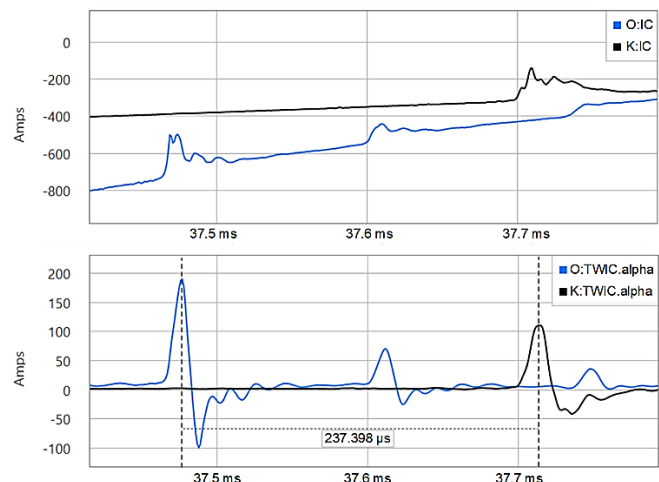


Fig. 17. C-phase alpha-mode current TWs that arrived at Omburu (O) and Khan (K) after being launched by a second arcing fault at the same fault location.

The second instance is observed 68 ms after the first fault initiated, when a clear reignition of the C-phase current is observed 108 μ s after an interruption at the previous current zero-crossing. The TWs launched at Omburu reflected from the fault and hit the open breaker at the Khan terminal. The details of these observations are shown in Fig. 18 and Fig. 19. By using the MHR (1 MHz sampling rate) IEEE COMTRADE record data, the UHS relays can also reveal transient phenomena, like breaker reignition. The relay can be used in a system to automatically detect, log, record, and alarm for breaker reignition detection [13]. Since circuit breakers interrupt fault current at the zero-crossing of the fault current, a reignition is likely to occur within 90 electrical degrees or less than 5 ms (for a 50 Hz system) of the zero-crossing. When a breaker reignition occurs, traveling waves are launched towards the fault location, which is still fully ionized, and then they travel to the remote terminal of the line. These TW reflections can be observed in the MHR IEEE COMTRADE record. This phenomenon caused a half-cycle delay while clearing the fault at Omburu.

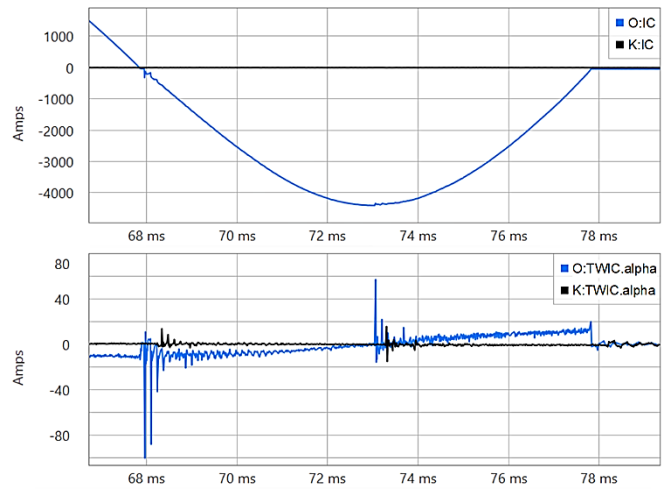


Fig. 18. C-phase currents and alpha-mode TWs at Omburu (O) and Khan (K) showing breaker reignition that delayed fault clearing by a half cycle.

As observed in Fig. 19, the difference in time between the TW launched at Omburu during the breaker reignition and received at Khan is 375.574 μ s, which is very close to the TWLPT value.

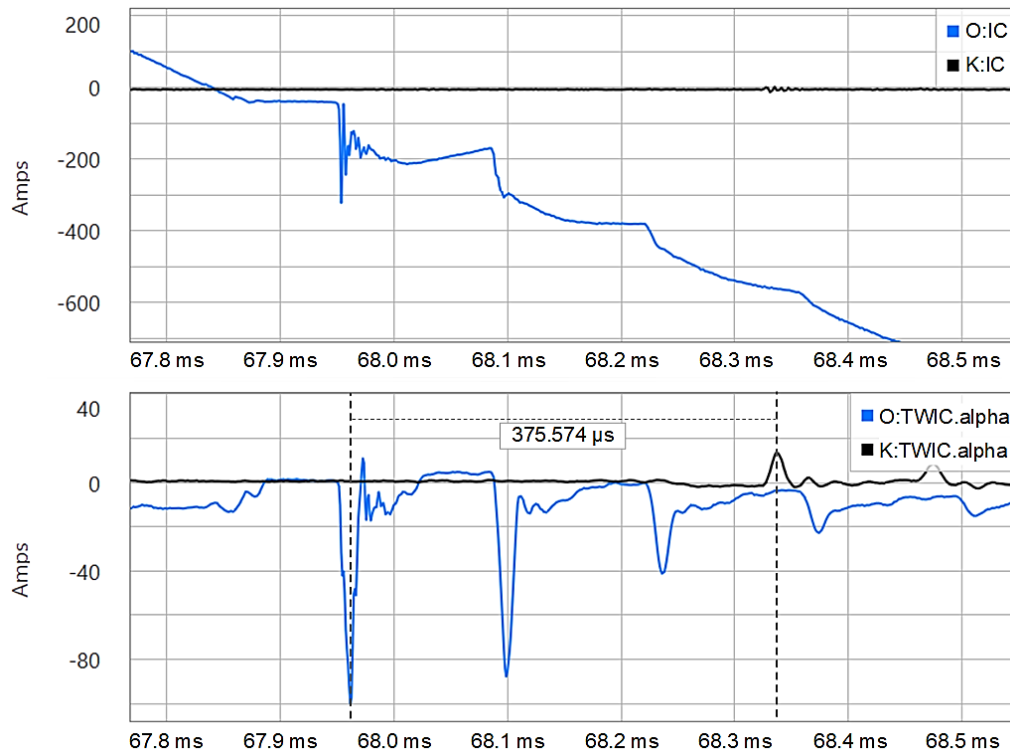


Fig. 19. Magnified view of C-phase current and alpha-mode TWs at Omburu (O) and Khan (K), showing breaker reignition shortly after a current zero-crossing and resulting in TWs traveling from Omburu and Khan.

VI. CONCLUSION

The use of TWs in line protective relays for UHS protection and accurate fault locating is gaining popularity. UHS relays with 1 MHz transient recording capabilities are providing valuable insights into power system operation. The field experience, observations, and lessons learned are similar and repeat those reported and documented by other users of UHS relays. These may be summarized as follows:

- The use of ultra-high-resolution recordings are invaluable in modern power systems highlighting significant issues, such as breaker reignition, post-fault arcing, lightning strikes, and many more.
- Enhancement in line protection performance from UHS relays compared to phasor-based relays is decisive when related to system stability and critical fault-clearing times, allowing more power transfer in the network.
- The TW87 scheme with direct fiber between the relays operates in around 1–2 ms using conventional current transformers; it is typically tenfold faster than phasor-based line differential schemes.
- The TW32 element speed (pickup in microseconds) and directional accuracy, combined with the dependability and security of the incremental-quantity directional TD32 element, significantly enhance the use and speed of POTT schemes [6].

UHS relays and the 20 ms (1 cycle at 50 Hz) reduction in FCT enables NamPower to assess improvements in power system transient stability margins, gain insight into equipment health, and take preventive action to reduce equipment wear. This insightful experience has ultimately endowed NamPower with the tools to proactively investigate and address potential problems, such as dielectric strength and quenching capability of the breaker, before they turn catastrophic [13]. With UHS relays, NamPower has the potential to further improve the reliability and availability indices of the transmission network to unprecedented levels.

VII. REFERENCES

- [1] NamPower, “NamPower Annual Report 2020,” 2020, Available: nampower.com.na/public/docs/annual-reports/NamPower%20Annual%20Report%202020.pdf.
- [2] E. O. Schweitzer, III, B. Kasztenny, A. Guzmán, V. Skendzic, and V. Mynam, “Speed of Line Protection – Can We Break Free of Phasor Limitations?” proceedings of the 41st Annual Western Protective Relay Conference, Spokane, WA, October 2014.
- [3] F. Albastri, T. Sidhu, and R. Varma, “Performance Comparison of Distance Protection Schemes for Shunt-FACTS Compensated Transmission Lines,” *IEEE Transactions on Power Delivery*, Vol. 22, Issue 4, October 2007.
- [4] *SEL-T400L Time-Domain Line Protection Instruction Manual*. Available: selinc.com/products/T400L/docs/.
- [5] E. O. Schweitzer, III, B. Kasztenny, and V. Mynam, “Performance of Time-Domain Line Protection Elements on Real-World Faults,” proceedings of the 42nd Annual Western Protective Relay Conference, Spokane, WA, October 2015.

- [6] A. Guzmán, V. Mynam, V. Skendzic, J. Eternod, and R. Morales, “Directional Elements – How Fast Can They Be?” proceedings of the 44th Annual Western Protective Relay Conference, Spokane, WA, October 2017.
- [7] B. Kasztenny, A. Guzmán, N. Fischer, V. Mynam, and D. Taylor, “Practical Setting Considerations for Protective Relays That Use Incremental Quantities and Traveling Waves,” proceedings of the 43rd Annual Western Protective Relay Conference, Spokane, WA, October 2016.
- [8] A. Guzmán, B. Kasztenny, Y. Tong, and V. Mynam, “Accurate and Economical Traveling-Wave Fault Locating Without Communications,” proceedings of the 44th Annual Western Protective Relay Conference, Spokane, WA, October 2017.
- [9] D. Corton, J. Melado, J. Cruz. Y. Korkmaz, G. Patti, and G. Smelich, “Double-Ended Traveling-Wave Fault Locating Without Relay-to-Relay Communications,” proceedings of the 74th Annual Conference for Protective Relay Engineers, Virtual Format, March 2021.
- [10] *SYNCHROWAVE Event Software Instruction Manual*. Available: selinc.com/products/5601-2/docs/.
- [11] B. Kasztenny and J. Rostron, “Circuit Breaker Ratings – A Primer for Protection Engineers,” proceedings of the 71st Annual Conference for Protective Relay Engineers, College Station, TX, March 2018.
- [12] Schweitzer Engineering Laboratories, Inc., “Field Experiences With Traveling-Wave Protection and Fault Locating,” Available: selinc.com/TW-Field-Experiences.
- [13] J. Matsuoka, “Use of a Protective Relay for Breaker Reignition Detection,” proceedings of the 46th Annual Western Protective Relay Conference, Spokane, WA, October 2019.
- [14] J. Grainger and W. Stevenson, Jr., *Power System Analysis*. McGraw-Hill Education, New York, NY, 1994.
- [15] R. Abboud and D. Dolezilek, “Time-Domain Technology – Benefits to Protection, Control, and Monitoring of Power Systems,” proceedings of the International Conference and Exhibition – Relay Protection and Automation for Electric Power Systems, April 2017.
- [16] C. Gross, *Power System Analysis*, John Wiley & Sons, Inc., Hoboken, NJ, 1986.
- [17] P. Kundur, *Power System Stability and Control*, McGraw-Hill Education, New York, NY, 1994.
- [18] H. Altuve, M. Thompson, and J. Mooney, “Advances in Breaker-Failure Protection,” proceedings of the 33rd Annual Western Protective Relay Conference, Spokane, WA, October 2006.

VIII. BIOGRAPHIES

Frans Shanyata is a senior engineer at Namibia Power Corporation (NamPower). He is currently leading a team of protection engineers within NamPower. As a team leader responsible for the protection of the NamPower transmission grid, his primary functions are in PAC schemes design, protection IED configuration and testing, and substation SCD files development. He is also responsible for transmission grid fault studies and analysis. He is a registered PE with the engineering council of Namibia. In 2010, Frans received his BE in electrical engineering; in 2012, he received his ME in high-voltage engineering and electrical physics from Kazan State Power Engineering University. He has been working for NamPower in the same field since 2013. He is also involved in CIGRE B5 working groups.

Shitaprajnyan Sharma received his BE in electrical engineering from Utkal University in 2006 and post-graduate diploma in international business from the Indian Institute of Foreign Trade in 2016. He has worked as a power system design engineer at SPML Infra Limited and as a protection engineer at ABB. He joined Schweitzer Engineering Laboratories, Inc. (SEL) in 2011 as a field application engineer and is currently working as an application engineering manager. He is involved in the training, technical support, and commissioning of protection and control solutions for generation, transmission, distribution, and industrial applications. He is an IEEE Power & Energy Society member since 2020 and a member of IET, UK. He is a registered professional engineer with the Engineering Council of South Africa.

Deon Joubert is the regional technical manager for Schweitzer Engineering Laboratories, Inc. (SEL), responsible for technical solutions and business development. He has 34 years of electric power engineering experience in transmission and distribution systems. In 1987, Deon graduated from Vaal University of Technology in heavy current electrical engineering. He was a senior design engineer in transmission design at Eskom (South Africa's national utility), developing feeder, bus zone, and transformer system designs. In 2000, he joined SEL as an international power system protection application engineer. In 2002, he transitioned to the role of regional manager and established the SEL office in South Africa for sales and customer services in the African region. He is a senior member of the South African Institute of Electrical Engineers and registered as a Professional Engineering Technologist with Engineering Council of South Africa. He is a member of the CIGRE Study Committee B5 Protection and Automation working group.

Richard Kirby is a senior product sales manager at Schweitzer Engineering Laboratories, Inc. (SEL) in Houston, Texas. His current focus is ultra-high-speed transmission line protection technology. He is a registered Professional Engineer in Arkansas, Louisiana, Michigan, Oklahoma, and Texas. He has 28 years of diverse electric power engineering experience. He received a BS in engineering from Oral Roberts University in 1992, and he earned his Master of Engineering in electric power from Rensselaer Polytechnic Institute in Troy, New York in 1995. He is an IEEE Power & Energy Society and Industrial Applications Society senior member.

Greg Smelich earned a BS in Mathematical Science and an MS in Electrical Engineering in 2008 and 2011, respectively, from Montana Tech of the University of Montana. Greg then began his career at Schweitzer Engineering Laboratories, Inc. (SEL) as a protection application engineer, where he helped customers apply SEL products through training and technical support, presented product demonstrations, worked on application guides and technical papers, and participated in industry conferences and seminars. In 2016, Greg made the transition to the SEL research and development division as a product engineer, where he now helps guide product development, training, and technical support related to time-domain technology. He has been a certified SEL University instructor since 2011 and an IEEE member since 2010. Greg is a registered professional engineer in the state of Washington.